2013 IEEE/RSJ International Conference on
Intelligent Robots and Systems (IROS)
November 3-7, 2013. Tokyo, Japan

Development of a Novel PCB-Based Voice Coil Actuator for Opto-Mechatronic Applications*

Nicholas Krouglicof, *Member, IEEE*, Michael Morgan, Nikhil Pansare, Taufiqur Rahman, and Dion Hicks

Abstract— **Voice-coil actuators are the simplest form of electric motor consisting of a non-commutated single coil or winding moving through a fixed magnetic field produced by stationary permanent magnets. From a system design point of view, however, it is generally the end user's responsibility to couple the voice-coil actuator with a linear bearing system, position feedback device, switch-mode or linear servo amplifier, and motion controller. The integration of multiple discrete components adversely affects system reliability and renders minimization and packaging difficult particularly when multiple actuators are required.**

In response to this demand, a novel, low-inertia voice coil actuator has been developed whereby the traditional moving coil is replaced with a printed circuit board (PCB) that incorporates the necessary windings as conductive traces on one or more layers of the board. The result is a compact, highly integrated, highly reliable design that is simple to mass-produce using conventional PCB manufacturing and assembly techniques.

I. Introduction

Current voice coil (i.e., linear electric) actuators are simple electromechanical devices that generate precise forces in response to an electrical input signal. Fundamentally they are the simplest form of electric motor consisting of a non-commutated single coil or winding moving through a fixed magnetic field produced by stationary permanent magnets[1] [2] [3]. Voice coil actuators are governed by the Lorentz force principle, which states that if a current-carrying conductor is placed in a magnetic field, then the magnitude of the force generated is $F = iL \times B$, where B is the magnetic flux density, L is the length of the conductor, and i is the current [4]. Because of the linear relationship between force and current, a voice coil actuator can be used for precise force control. The actuator itself is very reliable since no commutation is required for motion to occur.

From a system design point of view, it is generally the end-user's responsibility to couple the voice coil actuator with a linear bearing system, position feedback device, switch-mode or linear servo amplifier, and motion controller. The integration of multiple discrete components adversely affects system reliability and renders minimization and packaging difficult, particularly when multiple actuators are required.

For these reasons, in the proposed voice coil actuator design, the traditional moving coil is replaced with a printed circuit board (PCB) that incorporates the necessary windings as traces on multiple layers of the board. This approach has a number of advantages over traditional voice coil actuator designs. Firstly, the PCB has low moving mass, which allows for high accelerations of light payloads. Secondly, the use of conductive traces on multiple PCB layers provides a very compact design, in which the length of conductor can be increased easily, without adding bulk, by utilizing more PCB layers. Thirdly, PCBs with the required conductive traces can be produced cost effectively using conventional PCB manufacturing techniques. Finally, the signal conditioning and motion control electronics, position feedback device, and linear bearing system can be integrated on the same PCB, which reduces the size of the final system and leads to a more reliable design.

Another important feature of the proposed PCB-based voice coil actuator is the use of a modified Halbach array to provide a strong, substantially uniform interior magnetic field while ensuring the exterior field is near zero [2]. The array design is described in detail in Section II.A.

Typical applications of compact, short-stroke, precision voice coil actuators that are capable of high accelerations include *z*-axis positioning on pick and place machines, laser beam steering, mirror tilt and focusing, calibration of micro-electromechanical systems (MEMS) sensors, miniature position control, and precision opto-mechatronic systems.

The initial application of the PCB-based voice coil actuator is the development of a three degree-of-freedom parallel kinematic mechanism that can be used in place of current gimbal systems on unmanned vehicles, when the reliability, speed, positioning accuracy, size, weight and power (i.e.; SWaP) requirements of the sensor pointing device are critical. A typical application is tracking of fast-moving targets such as aircraft for sense-and-avoid in small, unmanned aerial vehicles.

II. System Components

A. Magnetics

An innovative adaptation to the Halbach array [5] was used to increase the static magnetic field interacting with the current flowing through the conductive traces of the PCB and to minimize the effects of the field in the immediate vicinity of the actuator. A typical Halbach array consists of magnets of equal size and strength arranged in alternating pole orientation [6]. The modified array consists of two opposing magnetic assemblies of five neodymium magnets of varying size. In order to help reduce the effects of the field on the surroundings and increase the interior field, magnetic stainless steel shielding was placed on the outside of the array.

*Research supported by the Boeing Company, the Atlantic Canada Opportunities Agency, and the Research & Development Corporation of Newfoundland and Labrador.

All authors are with the Faculty of Engineering and Applied Science, Memorial University of Newfoundland, St. John's, NL A1B 3X5 Canada (e-mail: {nickk, m.morgan, nikhil.pansare}@mun.ca).

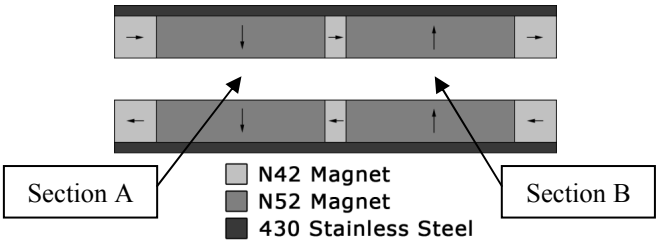

Fig. 1. Magnetic array and pole orientation

Large planar magnets in the vicinity of Section A and Section B are used to generate a strong, essentially uniform magnetic field of opposing polarity that is perpendicular to the conductive traces of the PCB. A smaller magnet separates them with its pole orienting the magnetic flux between the larger magnets. Smaller magnets on each end also direct the magnetic flux back into the device.

The magnetic array configuration was optimized through the use of the *Finite Element Method Magnetics* software package (FEMM Version 4.2). This software facilitates the visualization of various magnet configurations that affect the magnetic field strength and uniformity. Fig. 2 (below) provides a qualitative representation of the field strength and direction within the magnetic array. The field strength between the magnets is on the order of 0.7 Tesla (7,000 Gauss) while the field strength beyond the shielding is approximately two orders of magnitude lower. The FEMM results were later validated through experiments and are presented quantitatively in Section III.A.

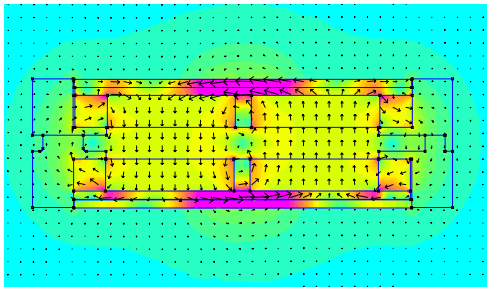
Fig. 2. FEMM voice coil actuator simulation

B. *Voice Coil Printed Circuit Board*

The novel voice coil actuator replaces the windings found in a conventional voice coil with traces on a PCB (Fig. 3). The benefits of this design include reduced weight and overall dimensions of the voice coil. Printed circuit boards have the option of multilayered traces that can quickly multiply the amount of force developed from a single PCB. The PCB also boasts the advantage of ease of production using conventional manufacturing techniques to produce the intricate trace patterns required with excellent repeatability. The thin nature of a PCB allows the two opposing magnet arrays to have a minimal spacing, increasing the magnetic field across the PCB.

Where more than one layer of windings are present within the PCB, it is important for the various layers to have the same orientation (clockwise versus counterclockwise), and as such, if one layer spirals inward, the next layer (from the perspective of the conductive trace) spirals outward.

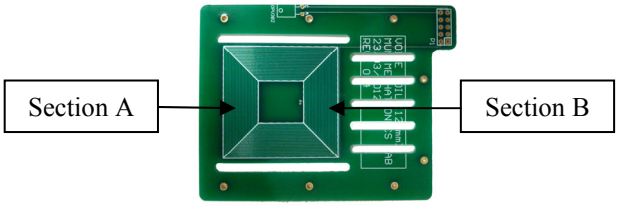

Fig. 3. Printed circuit board with coil

Note that the current in Section A of Fig. 3 flows in one direction while the current in Section B flows in the other direction. In order to take full advantage of the available length of conductor within the magnetic field, the magnetic field in the vicinity of Section A and Section B must be opposite over the operating range of the device. The modified Halbach array described in II.A provides a strong interior magnetic field of substantially uniform magnitude with polarity corresponding to the direction of current flow in the adjacent conductive traces on the PCB. In this fashion, the reversing magnetic field allows two different sections of the winding (i.e.; Sections A and B) to generate a force in the same direction thereby doubling the force constant of the actuator.

From a practical point of view, the voice coil PCB was manufactured using standard three ounce copper clad glass-reinforced epoxy laminate PCB material (FR-4) with 6 mil spaces and 14 mil traces. In the current design, this PCB technology yields approximately 1.36 meters of "useful" conductive traces per layer; i.e., conductive traces that contribute to the force constant. A four layer board has total of 5.44 meters of "useful" traces while an eight layer board has 10.88 meters. The overall thickness of the PCB is 1.5 mm for both the four and eight layer boards. While it would appear to be advantageous to increase the number of PCB layers indefinitely, maintaining tight tolerances on three ounce PCBs (i.e.; 105 µm copper thickness) with 6 mil spaces (i.e.; 152 µm) is technologically challenging beyond 8 layers. Note that the "valley" between conductive traces is approaching a square cross section (105 µm high by 152 µm wide).

C. *Guidance*

The voice coil printed circuit board is supported and accurately aligned through the use of commercially available miniature hardened steel rails and ball bearing carriages (manufactured by IKO Nippon Thompson Co., Ltd.). These provide a low-profile solution that enables the overall package to remain compact (refer to Fig. 4).

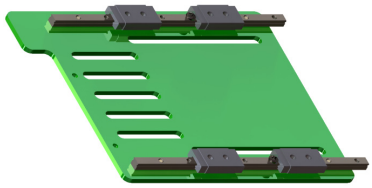
Fig. 4. Guidance system for the voice coil actuator

D. Feedback

To obtain high-resolution positioning accuracy, a one-dimensional (1D) position-sensitive device (PSD) and a vertical-cavity surface-emitting laser (VCSEL) diode were implemented. For the PSD, a Hamamatsu S3932 1D PSD was used, which provided an active range of 12 mm; whereas, for the VCSEL, an OPTEK Technology Inc. OPV382 diode was used, which provided a light spot with a diameter less than 200 µm. Combining this high-resolution sensor with a miniature, high-energy light spot, a signal conditioning circuit, and a 16-bit analog-to-digital converter (ADC) provides the potential for highly accurate positioning; a characteristic that is vital in opto-mechatronic applications.

PSDs are analog in nature and do not have a definable, geometric limit on resolution. Ultimately the resolution is photon or shot noise limited and can only be improved by increasing either the intensity of the light spot or the integration time. While the 16-bit ADC provides a maximum theoretical resolution of approximately 0.18 µm [i.e.; 12 mm/(2^{16} – 1)], the actual resolution obtained with an integration time of 300 µs was on the order of 0.8 µm (based on a 95% confidence limit). This is still exceptional in relation to comparable positioning devices [7] particularly when the moving mass of the sensor assembly is taken into account.

The PSD mentioned above functions by splitting the incident electromagnetic (i.e., light) energy into two photoelectric currents. The relative magnitudes of the two currents depend on the exact location of the incident light spot within the 12-mm active region. That is, the PSD's photosensitive layer can be treated as a material of uniform linear resistance; thus, based on the currents produced, the location of the light spot can be determined by the relationship given below [8].

$$x = k \cdot \frac{i_2 - i_1}{i_1 + i_2} \qquad (1)$$

Although the relationship given by (1) is relatively simple, from an analog computational point of view, the division by $i_1 + i_2$ poses a challenge. Despite the fact that analog division could be avoided by performing the necessary calculation within a digital controller, computational time can be reduced by eliminating this operation. Thus, as part of the signal conditioning electronics, the power output of the VCSEL diode was controlled through an integral control strategy such that $i_1 + i_2$ remained constant. This allowed for the position of the light spot to be measured without the need for an additional division operation.

The block diagram representation of the signal conditioning circuit for the PSD is shown in Fig. 5. The current-to-voltage converters with a first-order transfer function (i.e.; a time constant of 300 µs) convert the PSD photocurrents into voltages. After the conversion, a differential amplifier is used to compute the difference between the two voltages corresponding to the photocurrents; hence, the position of the incident light spot is calculated. As mentioned earlier, the sum of the two photocurrents is controlled at a constant value by varying the power to the VCSEL diode using a simple integral control loop.

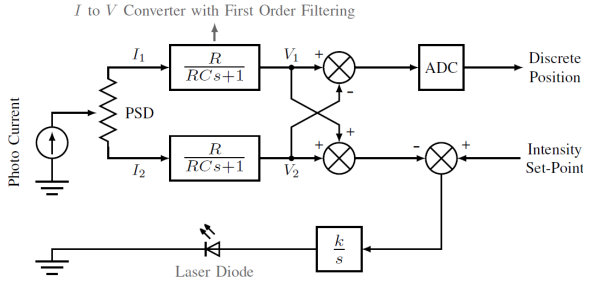

Fig. 5. Block diagram of PSD signal conditioning circuit

The PSD position feedback device with the associated signal conditioning and data acquisition electronics were integrated into the voice coil actuator and calibrated as unit against a precision linear gage (Mitutoyo LGF 0125L). The resolution of the linear gage was 0.1 µm while the absolute accuracy was 1.0 µm over a 10 mm range at 20 °C. The calibration results (Fig. 6) exhibited a coefficient of determination (i.e.; R^2 value) of 0.9999 for a simple, linear regression model.

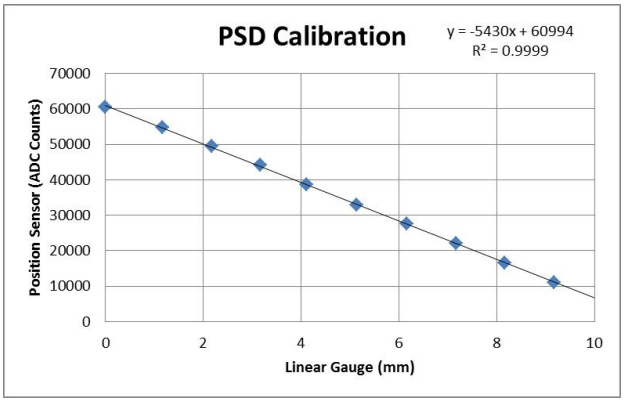

Fig. 6. Calibration of PSD sensor with signal conditioning circuit

The signal conditioning circuit and the separate circuit which provides power to the voice coil actuator were manufactured on miniature PCBs using surface-mount technology (SMT). The two PCBs are mounted on the actuator, as shown in the figure below. Thus, with the use of a high-resolution PSD sensor, appropriate signal conditioning electronics, and SMT, the design of a high-accuracy, compact feedback system was possible.

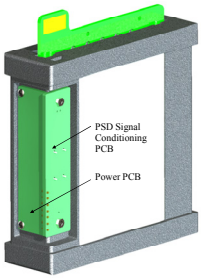

Fig. 7. PSD signal conditioning and power PCBs mounted on the actuator

III. Experimentation and Simulation

A. Magnetic Field Strength

To verify the magnetic field strength results provided by FEMM (refer to Section II.A), an experiment was devised in which the magnetic field strength of the modified Halbach array could be measured using a gauss meter and, subsequently, compared with theoretical results provided by FEMM. The set-up for this experiment is shown in Fig. 8 below. As seen in the figure, a gauss meter probe was inserted between the two magnetic arrays of the actuator and was accurately positioned using a digital dial indicator.

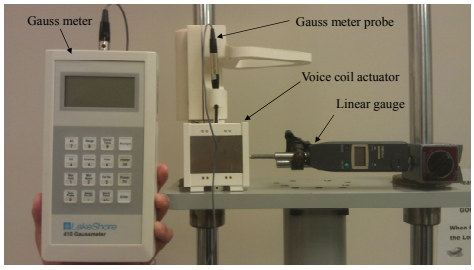

Fig. 8. Experimental set-up for magnetic field strength test

The field strength was measured at 0.1 inch intervals along the central axis through the length of the array. Upon acquiring the experimental data, they were compared with FEMM results, as shown in Fig. 9 below. As can be seen in the plot, experimental results matched well with those provided by FEMM, and the modified Halbach array was indeed found to be producing the expected magnetic field.

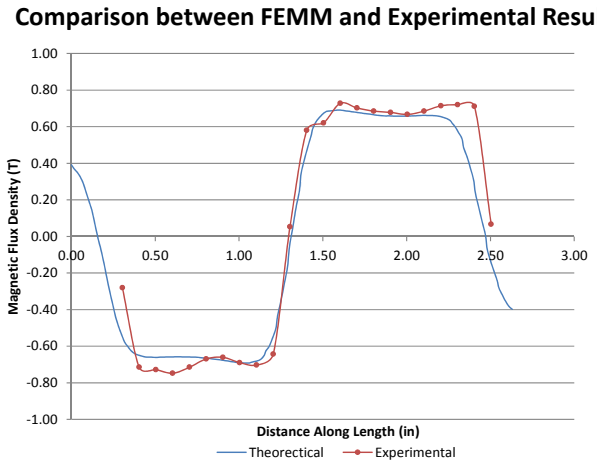

Fig. 9. Comparison between FEMM and experimental results

B. Thermal Experimentation and Modeling

When designing any mechatronic device, the thermal limitations of the various sub-systems within the device must be considered. That is, in the case of the voice coil actuator, it was desired to keep the temperature of the voice coil PCB below 70 °C to avoid damaging the PCB as well as the magnetic arrays which must remain below 80 °C to prevent the onset of demagnetization [9]. Thus, a thermal model of the voice coil actuator was developed for predicting the transient and steady-state thermal responses of the voice coil PCB and the magnetic arrays for a reasonable range of input currents.

To obtain the necessary data for thermal modeling, two sets of experiments were performed. More specifically, two orientations of the voice coil actuator were tested (see Fig. below); each orientation was tested at current levels of 0.25 A, 0.50 A, and 0.75 A.

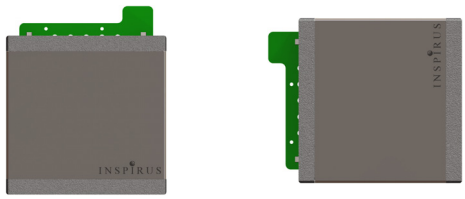

Fig. 10. "Vertical" (left) and "side" (right) orientations of the voice coil actuator

To conduct the experiments, a Type K thermocouple, connected to signal conditioning electronics and a 16-bit analog-to-digital converter (ADC), was used. The temperature readings of the voice coil PCB and the magnetic array were recorded at a frequency of 1 Hz on a personal computer.

After experimentation, a simple second-order, lumped-parameter thermal model of the voice coil actuator was developed based on material properties and the data obtained from the experiments. The thermal model is shown graphically in Fig. 11 below and the various parameters shown in the figure are detailed in Table I.

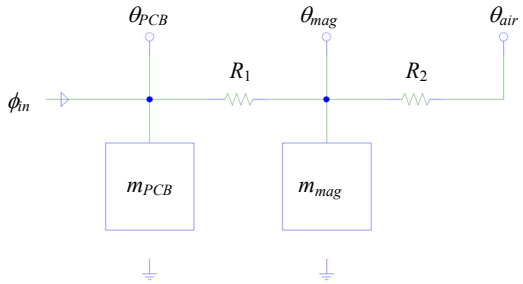

Fig. 11. Second-order, lumped-parameter thermal model of the voice coil actuator

TABLE I. Parameters in Thermal Model

Symbol	Description	Units
ϕ_{in}	Voice coil power input	[W]
θ_{PCB}	Voice coil average temperature	[°C]
θ_{mag}	Magnetic array average temperature	[°C]
θ_{air}	Ambient air temperature	[°C]
R_1	Voice coil-magnetic array average thermal resistance	[°C/W]
R_2	Magnetic array-air average thermal resistance	[°C/W]
m_{PCB}	Voice coil thermal mass	[J/°C]
m_{mag}	Magnetic array thermal mass	[J/°C]

Upon acquiring the data from the six experiments described earlier, the thermal resistance parameters (i.e., R_1 and R_2) were approximated by comparing experimental results with those from the model. To facilitate the comparison process, a Simulink block diagram of the thermal model was made using the governing ordinary differential equations of the system, which are given below:

$$\dot{\theta}_{PCB} = \frac{\phi_{in}}{m_{PCB}} - \frac{1}{R_1 m_{PCB}}(\theta_{PCB} - \theta_{mag}) \quad (2)$$

$$\dot{\theta}_{mag} = \frac{1}{R_1 m_{mag}}(\theta_{PCB} - \theta_{mag}) - \frac{1}{R_2 m_{mag}}(\theta_{mag} - \theta_{air}) \quad (3)$$

The results of the thermal model, overlaid with corresponding experimental results, are shown in Fig. 12. The thermal mass[1] and thermal resistance parameters used in the model were R_1 = 8.0 °C/W, R_2 = 11.5 °C/W, m_{PCB} = 18 J/°C, and m_{mag} = 170 J/°C. It should be noted that, from the experimental results, it was found that both orientations of the voice coil actuator could be modeled using the same thermal parameters. From the figure, it can be seen that the thermal model accurately predicted the voice coil PCB and temperatures.

Based on experimental and model results, it was found that, in order to prevent damage to the voice coil PCB, the maximum continuous current could be no greater than 0.5 A. At this current, the temperature of the voice coil reached approximately 65 °C, a temperature sufficiently close to the allowable limit of 70 °C. Note that, at this current, the magnetic array temperature was approximately 54 °C, which was well below the demagnetization onset temperature of 80 °C mentioned earlier.

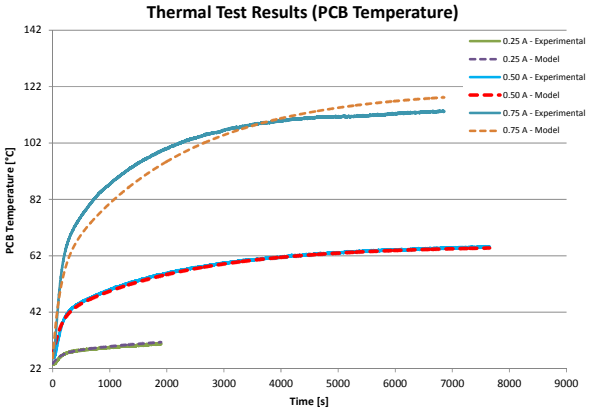

Fig. 12. Experimental results vs. model results for the voice coil PCB temperature

C. Force Constant

One of the key parameters that define a linear actuator's performance is its motor, or force constant. This parameter allows one to predict the additional force generated by the actuator for every unit increase in current. To measure the actuator's force constant, a simple experiment was performed in which weights were attached to the voice coil PCB, and the current required to lift each weight was measured and recorded.

Upon acquiring the data, the results of the experiment were plotted with the voice coil current displayed on the abscissa and the total weight[2] displayed on the ordinate (Fig. 13). From the experiment, a value of approximately 3.3 N/A was determined for the voice coil actuator's force constant. Based on theoretical calculations, a value of 3.8 N/A was predicted for the force constant. These calculations were based on the length of "useful" conductor within the magnetic field as well as the field strength. Thus, the experimental value was indeed reasonable, but may have differed from the theoretical value due to uncertainties associated with the exact 3D magnetic field distribution within the actuator.

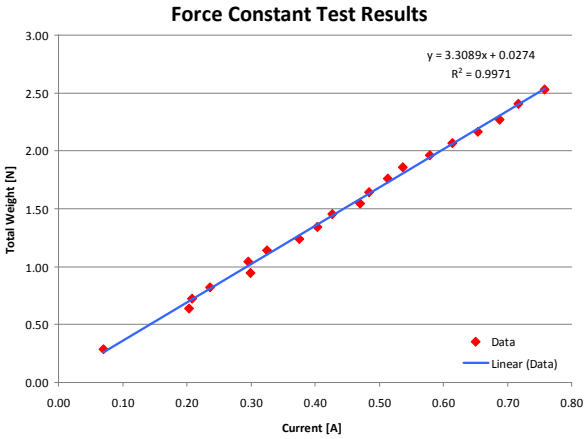

Fig. 13. Force constant test results

D. Static Friction

One limitation to linear actuators is the amount of friction produced by the guidance system. In order to determine the amount of friction developed by the linear bearings, a test assembly was developed (see Fig. 14). The test assembly used an optical encoder to accurately measure the angle of the actuator at the point at which the PCB overcame static friction. Results from the test indicated that the coefficient of static friction of the assembled voice coil actuator is approximately 0.500. This was deemed consistent using statistical analysis, showing that the standard deviation was approximately 0.070, with a 95% confidence interval range of ±0.020.

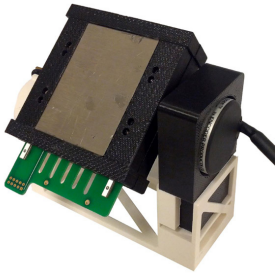

Fig. 14. Static friction coefficient test assembly

[1] The thermal masses of the voice coil PCB and magnetic arrays were both approximated using the specific heat capacity and total mass of the respective components.

[2] Total weight included the moving weight of the voice coil actuator as well as the added weight.

IV. Performance Summary of the Voice Coil Actuator

The key specifications and performance parameters associated with the voice coil actuator are summarized in Table II below. These data allow for comparison between the PCB-based actuator described thus far and commercially available voice coil actuators. An exploded view of the actuator is also given in Fig. 15. The table beneath the figure details the numbered components in the exploded view.

TABLE II. General Specifications

Parameter	Value
Height	102 mm (fully extended)
	90 mm (fully retracted)
Width	82.8 mm
Depth	25.4 mm
Total mass	656 g
Moving mass	27.4 g
Stroke	12.0 mm (nominal)
Force constant	3.31 N/A
Back EMF constant	3.31 V·s/m
Static friction coefficient	0.500
Coil resistance	8.70 Ω (typical)
Coil inductance	327 μH (typical)
Magnetic flux density	0.704 T (typical)
Voice coil thermal mass	18.0 J/°C
Magnetic array thermal mass	170 J/°C
Voice coil-magnetic array thermal resistance	8.00 °C/W (average)
Magnetic array-air thermal resistance	11.5 °C/W (average)

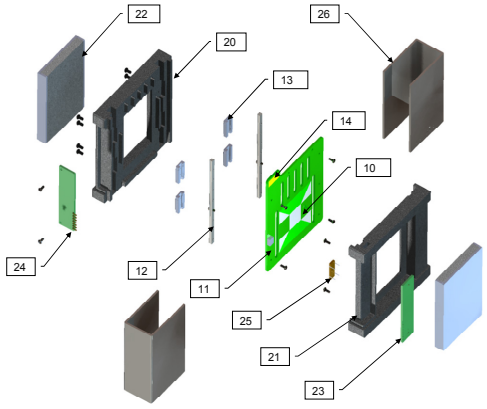

Fig. 15. Exploded view of voice coil actuator

TABLE III. Components in Exploded View

Number	Description	Quantity
10	Voice coil PCB	1
11	Laser diode	1
12	Linear bearing guide rail	2
13	Linear bearing carriage	4
14	Electrical connector	1
20	Exterior magnet holder	1
21	Interior magnet holder	1
22	Modified Halbach array	2
23	Signal conditioning PCB	1
24	Power PCB	1
25	1D PSD	1
26	Steel jacket	2

A. Dynamic Model

Using the system parameters determined through direct measurement (e.g.; coil impedance) and experimentation (e.g.; force constant, coulomb friction), a MATLAB-Simulink model was created in order to simulate the dynamics of the voice coil actuator (Fig. 16). The model is that of a simple linear motor. That is, to determine the current, the applied voltage is first reduced by the back electromotive force and, subsequently, divided by the coil impedance. The net force is then obtained by incorporating the force constant and the friction coefficient. Acceleration is then obtained through division by the moving mass. Lastly, velocity and position are determined by integration.

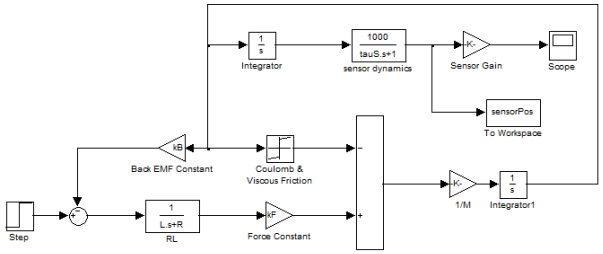

Fig. 16. Voice coil actuator sub-system

From this model, the open-loop, no-load system response to step inputs of 8, 16, and 24V were obtained and compared with experimental data (Fig. 17). In each case, there is an excellent correlation between the dynamic model and the experiments with the dynamic model responding slightly slower than the actual system. It is worth noting that with no load, the actuator is capable of accelerations in excess of 30 g and peak velocities in excess of 2 m/s. This is largely unprecedented for an actuator of this type.

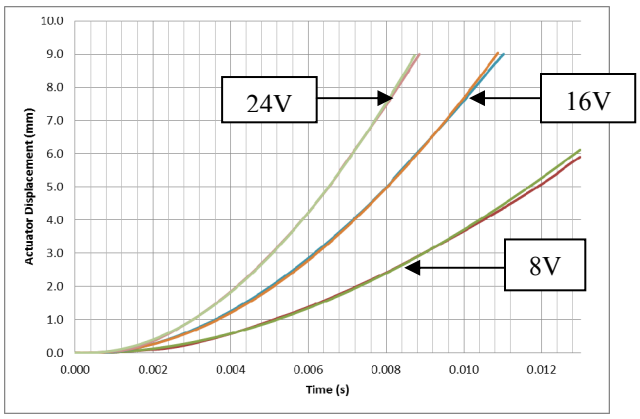

Fig. 17. Open loop response of voice coil actuator to a step input

The closed loop performance of the actuator was evaluated by incorporating a simple proportional-derivative (PD) controller with position feedback as provided by the PSD and associated signal conditioning circuit (Fig. 18). Note that an integral term was not deemed necessary in this simple controller since the type number of the voice coil actuator is one under displacement control.

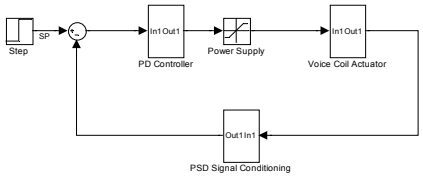

Fig. 18. Model of voice coil actuator with PD controller and feedback

The no-load response of the closed-loop system to a step input corresponding to a displacement of 6 mm is illustrated in Fig. 19. The rise and settling times are on the order of 7 and 15 ms respectively. Current work is focused on developing a more robust control strategy based on an Automatic Disturbance Rejection Controller (ADRC).

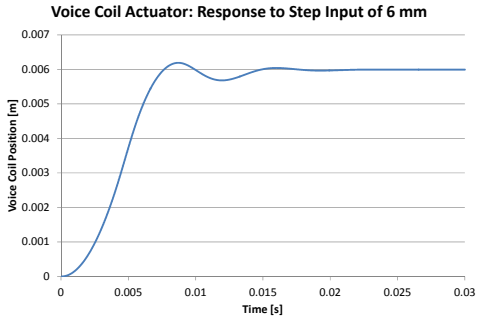

Fig. 19. Response of voice coil actuator for 6-mm step input

V. Conclusion

By approaching the design of a voice coil in a novel manner, a unique, low-inertia linear actuator has been developed. The designed actuator is relatively compact and has a moving mass of less than 30 grams. Furthermore, the actuator is capable of providing a force constant of over 3 N/A and maximum velocity and acceleration values of 2.0 m/s and 30g respectively; this is a significant accomplishment, especially for an actuator of this size. Lastly, the guidance system employed in the actuator provides low-resistance motion, with a static friction coefficient of 0.500 and a kinetic friction coefficient of even lower magnitude. Thus a compact, highly integrated, highly reliable voice coil actuator has been developed that is simple to mass-produce using conventional PCB manufacturing and assembly techniques.

Acknowledgment

A special thanks is due to Dr. Kaaren May for providing valuable feedback regarding the presentation of the paper. In addition, the authors wish to thank Matthew Roberts, Levi MacNeil, and Indra Sarwinata, the previous students that worked on the development and testing of the voice coil actuator. Lastly, the authors thank Tom Pike, Brian Pretty, Steve Steele, and Don Taylor for their valuable advice during design and testing of the actuator.

References

[1] F. Baronti, A. Lazzeri, F. Lenzi, R. Roncella, R. Saletti, and S. Saponara, "Voice Coil Actuators: From Model and Simulation to Automotive Application," *35th Annual IEE Conference on Industrial Electronics (IECON'09)*, 2009, pp. 1805-1810.

[2] W. Robertson, B. Cazzolato, and A. Zander, "Parameters for Optimizing the Forces Between Linear Multipole Magnetic Arrays," *IEEE Magnetic Letters*, Vol. 1., 2010.

[3] X.M. Feng, Z.J. Duan, Y. Fu, and A.L. Sun, "The technology and Application of Voice Coil Actuator," *2nd International Conference on Mechanical Automation and Control Engineering (MACE)*, 2011, pp. 892-895.

[4] D. C. Karnopp, D. L. Margolis, and R. C. Rosenberg, *System Dynamics: Modeling and Simulation of Mechatronic Systems*, 4th ed. John Wiley & Sons, Inc., 2006.

[5] S. Dwari and L. Parsa, "Design of Halbach-Array-Based Permanent-Magnet Motors with High Acceleration," *IEEE Transactions on Industrial Electronics*, Vol. 58, No. 9, September 2011, pp. 3768-3775.

[6] J. Wang, C li, Y. Li, and L Yan, "Optimization Design of Linear Halbach Array," *International Conference on Electrical Machines and Systems (ICEMS 2008)*, 2008, pp. 170-174.

[7] T. Villgrattner, R. Zandert, and H. Ulbrich, "Modeling and Simulation of a Piezo-Driven Camera Orientation System," *Proceedings of the 2009 IEEE International Conference on Mechatronics (ICM 2009)*, Malaga, Spain, April 2009.

[8] (2011, April). *One-dimensional PSD: S3931, S3932, S3270*. Hamamatsu Photonics K.K. [Online: http://sales.hamamatsu.com]

[9] (2012, September 8). *Neodymium Magnet Information*. K&J Magnetics, Inc. [Online: http://www.kjmagnetics.com]